DR2009069

Analytical techniques

The structural characterization of graphite from the Borrowdale deposit has been carried out by means of X-ray diffraction (XRD) and Raman spectroscopy. For the XRD study, after grinding and homogenization to <53 μm, ten samples of randomly orientated powders of graphite were run in a Siemens D-500 diffractometer, using Cu-Kα radiation at 30 kV and 40 mA, a step size of 0.03 (º2θ), a slit system of 1º-1º-1º-0.15º, and time per step of 1 s (scan rate of 1.8º 2θ/min). Each sample was run at least twice using silicon as the internal standard. Measurements on the XRD patterns were done using the Diffrac Plus EVA 10.0 software.

Raman spectra were collected with the Renishaw INVIA equipment at the Ecole Normale Superieure (Paris, France) on polished thin sections used for the petrographic study. A total of 60 measurements were obtained focusing the laser beam on graphite located beneath the surface of adjacent transparent minerals (usually quartz, chlorite, and epidote) to avoid the effect of polishing at the surface of the thin section which may alter the graphite structure (Pasteris, 1989; Beyssac et al., 2003). The 514.5 nm wavelength of a 20 mW Spectra Physics Argon laser focused through a 100x objective (N.A.=0.90) was used for the analyses. Under these conditions the spatial resolution is ~1 μm and the spectral resolution is close to 1 cm^{-1}. Laser power on the sample surface was reduced to 2 mW to avoid radiation damage to the graphite. Raman analysis of graphite also might be affected by polarization effects between the incident laser electromagnetic field and the structure of graphite, and this might virtually enhance the defect bands especially for measurement on the graphite edge planes. These effects are rather weak with a 514.5 nm wavelength (Tan et al., 2004), and to further attenuate them we used a ¼ wavelength plate before the microscope which yields a circular polarization of the laser. The Raman parameters (peak position, band intensity, and band area) were determined with the computer program PeakFit 3.0 using a Voigt function.

The microthermometric study of the fluid inclusions was carried out using a Linkam THMSG 600 heating and freezing stage at the Department of Crystallography and Mineralogy, Universidad Complutense, Madrid. Raman analysis of the volatile fraction was also performed at the Ecole Normale Superieure under the same analytical conditions given above, but the laser power in this case was 50 mW. Bulk composition,

density and molar volume of the inclusions were calculated with the computer programs DENSITY, ICE and BULK, versions 12/02 (Bakker and Brown, 2003) using the Duan et al. (1992a,b) equation of state and considering NaCl as the only salt in solution.

Fluid inclusions data

Fluid inclusions were studied in quartz fragments hosted by the graphite nodule-bearing pipes (Figure DR1). The angular shape of these fragments and their internal grainy texture indicate that the quartz was brecciated, pulled up from its original location and transported upwards within subvertical structures favoured by a fluid-rich regime that eventually resulted in the precipitation of huge amounts of graphite. These fluids were recorded as secondary fluid inclusions in the quartz xenoliths. Three types of secondary fluid inclusions have been recognized, based upon appearance at room temperature and microthermometric behaviour:

Type V. Two-phase vapour-rich inclusions (Vv/Vt = 60-90%), made up by H_2O-CO_2- CH_4. These inclusions are very abundant and occur along trails within the clear cores of the quartz grains. Raman data of the volatile fraction indicate mixtures of CO_2-CH_4, with XCO_2 between 0.6-0.75. The average bulk composition (mol fraction) of these inclusions is 0.65 H_2O, 0.24 CO_2, 0.11 CH_4 and 1.4 wt% NaCl, with a $XCO_2/(XCO_2+XCH_4)$ ratio of 0.69 and an average molar volume of 40 $cm^3.mol^{-1}$. Total homogenization of the inclusions ranges 295-340 ºC (into vapour) and 328-350 ºC (critical behaviour) indicating that the fluid would be a vapour-like supercritical phase at the trapping conditions. Complete microthermometric and compositional data of selected type V inclusions can be found in Table DR1.

Type L1. Two-phase liquid-rich H_2O-CO_2- CH_4-bearing inclusions (Vv/Vt = 25-40%). These inclusions are very scarce and occur spatially associated with type V inclusions. Raman analysis indicates XCO_2 between 0.03-0.28 in most L1 inclusions (n=6) and only two specimens with XCO_2=0.6-0.62. Bulk composition (mol fraction), calculated only in one inclusion due to the difficulty of measuring clathrate melting, is estimated to be 0.916 H_2O, 0.018 CO_2, 0.022 CH_4 and 0.044 NaCl (7.2 wt% NaCl), with a $XCO_2/(XCO_2+XCH_4)$ ratio of 0.45 and a molar volume of 25 $cm^3.mol^{-1}$. Total homogenization occurs between 279 and 378 ºC, in a range which is similar to homogenization temperatures for type V inclusions. However, whereas type V homogenizes either by bubble expansion or show critical behaviour, L1 inclusions always homogenize into liquid.

Type L2. Two-phase liquid-rich inclusions (Vv/Vt < 10%). They are very abundant and occur along trails that occasionally cross-cut quartz grain boundaries, thus indicating that the inclusions are secondary in origin and postdate the type V and L1 fluid circulation. They also occur in recrystallized boundaries of the quartz grains, probably as primary inclusions. CH_4 is the only carbonic species in these inclusions, with an estimated average composition of 0.93 H_2O, 0.02 CH_4 and 0.05 NaCl. Melting of ice occurs in the range -6 to -2.8 ºC and indicates salinities between 4.5 and 9.5 wt% NaCl. The total homogenization of the L2 inclusions occurs between 123 and 204 ºC, with a maximum in the interval 180-190 ºC.

These fluid inclusions assemblages have been interpreted to be the record of the evolution of the carbon-bearing fluids involved in the pipes' development and the subsequent graphite deposition. In this scenario, the type V vapour-rich fluid would be the fluid circulating at the earliest stages of the process just before graphite saturation was reached. Therefore, the physicochemical parameters estimated from this fluid would indicate the initial P-T-fO_2 conditions of the graphite forming system which are the aim of this paper.

References cited

Bakker, R.J., and Brown, P.E., 2003, Computer Modelling in Fluid Inclusion Research, in Samson, I., Anderson, A., and Marshall, D., eds., Fluid Inclusions: Analysis and Interpretation. Mineralogical Association of Canada, Short Course series, v. 32, p. 175–212.

Beyssac, O., Goffé, B., Petitet, J.P., Froigneux, E., Moreau, M., and Rouzaud, J.-N., 2003, On the characterization of disordered and heterogeneous carbonaceous materials by Raman spectroscopy. Spectrochimica Acta, Part A, v. 59, p. 2267-2276.

Duan, Z., Møller, N., and Weare, J.H., 1992a, An equation of state for the CH4-CO2-H2O system: I. Pure systems from 0 to 1000 ºC and 0 to 8000 bar: Geochimica et Cosmochimica Acta, v. 56, p. 2605–2617, doi: 10.1016/0016-7037(92)90347-L.

Duan, Z., Møller, N., and Weare, J.H., 1992b, An equation of state for the CH4-CO2-H2O system: II. Mixtures from 50 to 1000 ºC and 0 to 1000 bar: Geochimica et Cosmochimica Acta, v. 56, p. 2619–2631, doi: 10.1016/0016-7037(92)90348-M.

Pasteris, J.D., 1989, In situ analysis in geological thin-sections by Laser Raman Microprobe Spectroscopy: a cautionary note. Applied Spectroscopy, v. 43, p. 567-570.

Tan, P.H., Dimovski, S., and Gogotsi Y., 2004, Raman scattering of non-planar graphite: arched edges, polyhedral crystals, whiskers and cones. Philosophical Transactions of the Royal Society of London, part A, v. 362, p. 2289-2310, doi: 10.1098/rsta.2004.1442.

TABLE DR1. MICROTHERMOMETRIC, RAMAN AND CALCULATED COMPOSITIONAL DATA OF SELECTED TYPE V INCLUSIONS FROM THE BORROWDALE DEPOSIT

	Non aqueous phase data						Bulk inclusion data						
Vv/Vt	**$TmCO_2$**	**$ThCO_2$**	**TmCl**	**XCO_2**	**XCH_4**	**Molar volume**	**XH_2O**	**XCO_2**	**XCH_4**	**Salinity**	**TH**	**Bulk molar volume**	**#XCO_2**
0.8	-58.4	+1.5 L	+14.2	0.64	0.36	75.43	0.49	0.33	0.18	3.03	294 *	46.50	0.65
0.5	-57.4	+8.9 L	+14.2	0.75	0.25	75.52	0.78	0.17	0.05	0.47	340 C	29.66	0.43
0.7	-	+3.8 L	+14.2	0.75	0.25	77.29	0.63	0.28	0.09	0.28	300 *	39.50	0.76
0.7	-	-8.1 L	+14.2	0.60	0.40	86.52	0.64	0.21	0.13	2.86	295 *	40.90	0.62
0.7	-58.7	-1.9 L	+14.4	0.67	0.33	81.78	0.64	0.25	0.11	1.36	293 *	40.21	0.69
0.7	-	+3.3 L	+14.2	0.75	0.25	76.16	0.62	0.29	0.09	0.4	318 V	39.30	0.76
0.6	-61.8	+5.1 L	+14.2	0.69	0.31	74.99	0.71	0.20	0.08	2.02	340 V	33.62	0.71
0.9	-	+4.1 L	+14.2	0.68	0.32	75.83	0.0024	0.768	0.23	-	322 V	84.26	0.77

Molar volume in $cm^3.mol^{-1}$, salinity in eq. NaCl wt%, temperature in ºC. Vv/Vt: bubble volume fraction, X: molar fraction, Tm: melting temperature, Th: partial homogenization temperature, TH: total homogenization temperature, Cl: clathrate, $\#XCO_2 = XCO_2/(XCO_2+XCH_4)$, * Decrepitation temperature before homogenization, C: critical homogenization, L: homogenization into liquid, V: homogenization into vapour.

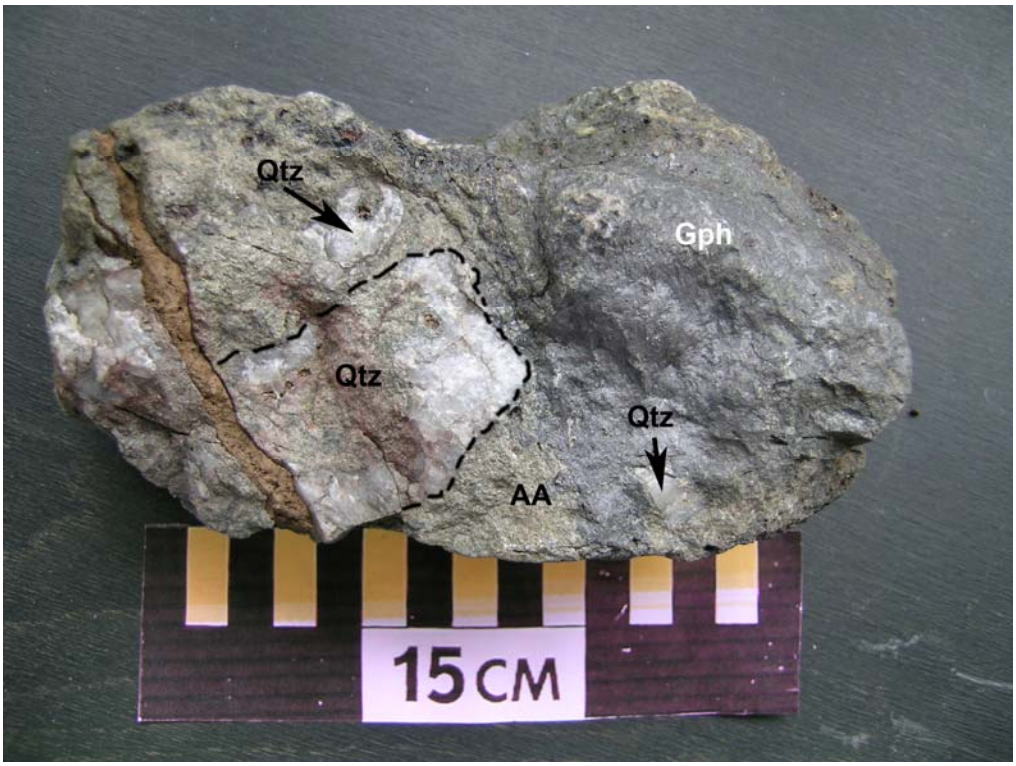

Figure DR1. Hand specimen of the common graphite-quartz association from the Borrowdale deposit. Note the large angular quartz fragment (Qtz), and the intense alteration of the andesite host rock (AA). Small quartz fragments are also embedded within the graphite mass (Gph).

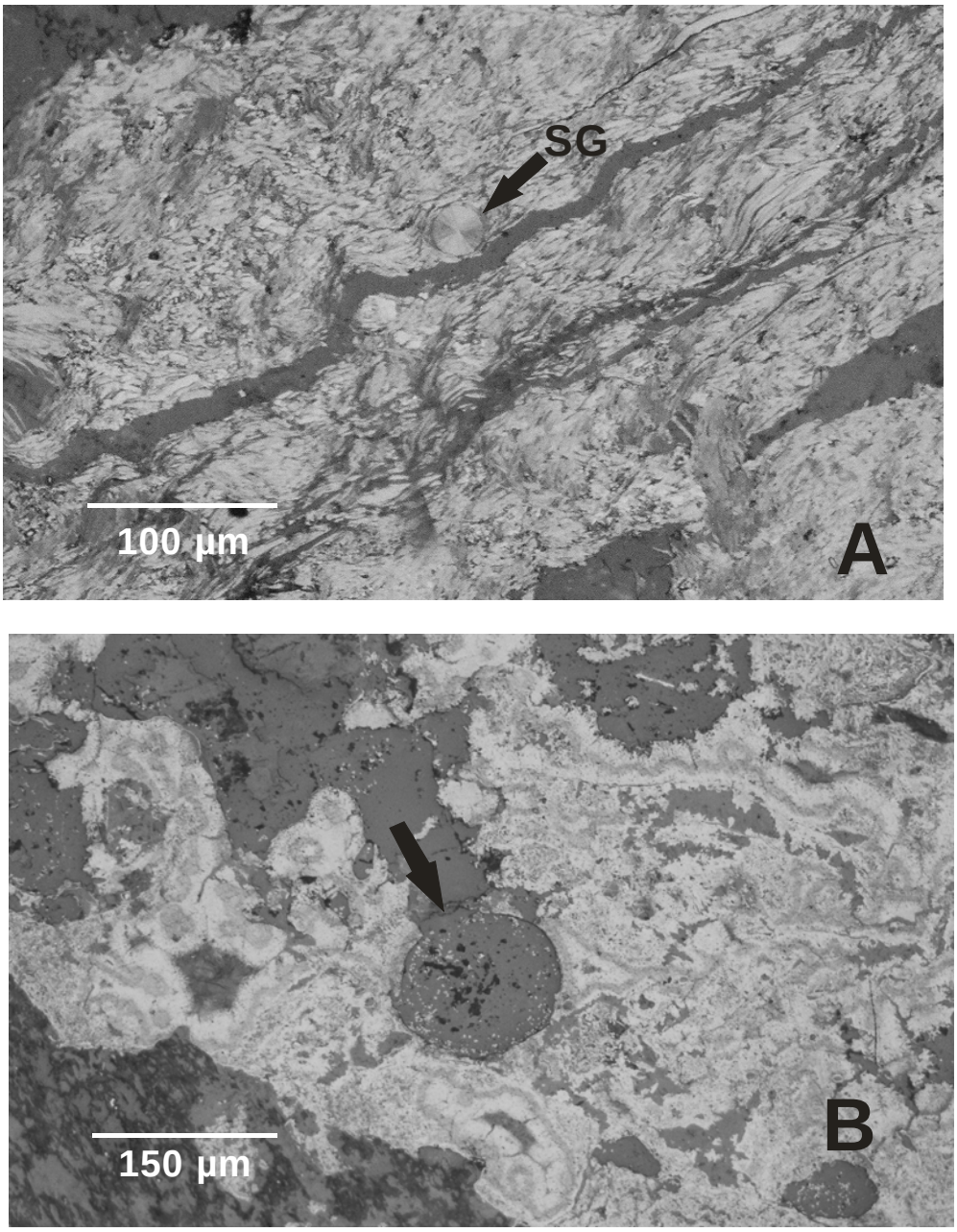

Figure DR2: Reflected light photomicrographs (one polar) of graphite morphologies from the Borrowdale deposit. A) Spherulitic graphite (SG) within flaky graphite. B) Cryptocrystalline graphite with colloform texture enclosing quartz grains. The arrow indicates a rounded quartz grain containing minute spherulites of graphite.

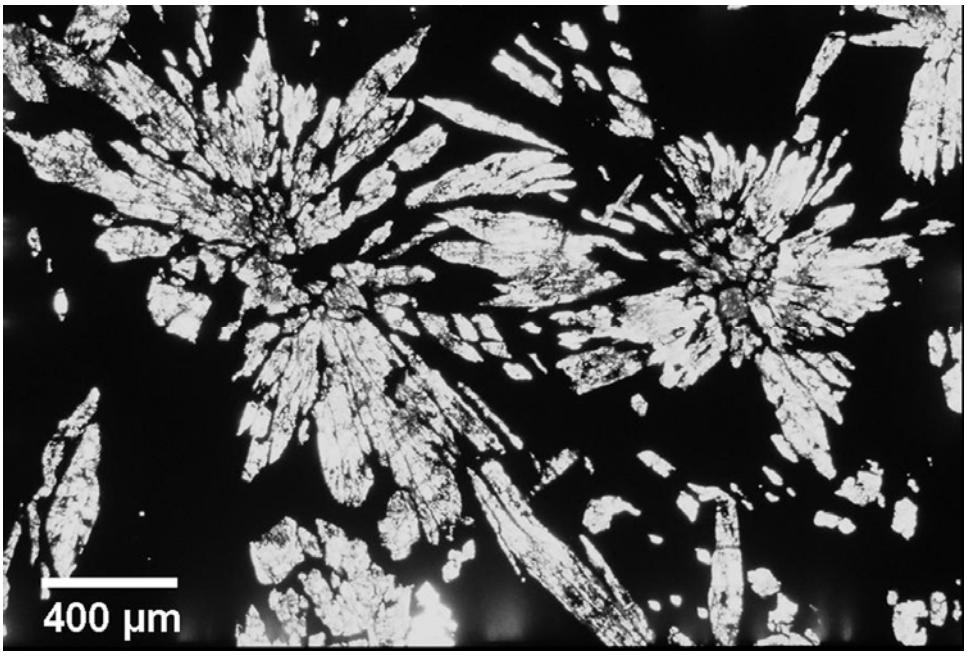

Figure DR3: Transmitted light photomicrograph showing radial aggregates of epidote crystals within a graphite (in black) nodule.